Internal transport barriers in NSTX

H. Y. Yuh,[1] R. E. Bell,[2] J. C. Hosea,[2] S. M. Kaye,[2] B. P. LeBlanc,[2] F. M. Levinton,[1] E. Mazzucato,[2] J. L. Peterson,[2] D. R. Smith,[2] J. Candy,[3] C. W. Domier,[4] W. Lee,[5] N. C. Luhmann Jr.,[4] H. K. Park,[5] and R. E. Waltz[3]

[1] *Nova Photonics Inc., Princeton, New Jersey 08540, USA**
[2] *Princeton Plasma Physics Laboratory, Princeton University, Princeton, New Jersey 08543, USA*
[3] *General Atomics, San Diego, California 92186-5608, USA*
[4] *University of California at Davis, Davis, California 95616, USA*
[5] *POSTECH, Pohang 790-784, Korea*

(Dated: December 5, 2008)

In the National Spherical Torus eXperiment (NSTX), internal transport barriers (ITBs) are observed in reversed (negative) shear discharges where diffusivities for electron and ion thermal channels and momentum are reduced. While neutral beam heating can produce ITBs in both electron and ion channels, High Harmonic Fast Wave (HHFW) heating can also produce electron ITBs (e-ITBs) under reversed magnetic shear conditions without momentum input. Interestingly, the location of the e-ITB does not necessarily match that of the ion ITB (i-ITB). The e-ITB location correlates best with the magnetic shear minima location determined by Motional Stark Effect (MSE) constrained equilibria, whereas the i-ITB location better correlates with the location of maximum $\mathbf{E}\times\mathbf{B}$ shearing rate. Measured electron temperature gradients in the e-ITB can exceed critical gradients for the onset of ETG microinstabilities calculated by linear gyrokinetic codes. A high-k microwave scattering diagnostic shows locally reduced density fluctuations at wavenumbers characteristic of electron turbulence for discharges with strongly negative magnetic shear versus weakly negative or positive magnetic shear. Reductions in fluctuation amplitude are found to be correlated with the local value of magnetic shear. These results are consistent with nonlinear gyrokinetic simulations predicting a reduction of electron turbulence in negative magnetic shear conditions despite exceeding critical gradients.

INTRODUCTION

Understanding the underlying mechanisms that lead to improved plasma confinement in internal transport barriers (ITBs) has been a continous topic of interest in magnetic fusion research, because ITBs have the potential to become a powerful tool much like the H-mode edge transport barriers. Improved confinement resulting from ITBs have been previously reported on many tokamaks, with a multi-machine review found in [1], and also more recently in a spherical torus [2]. Here we report on measurements of ITBs in the National Spherical Torus eXperiment (NSTX), where improved confinement for reversed shear plasmas is observed simultaneously in the electron and ion thermal channels, as well as in toroidal velocity. Calculated thermal diffusivities inside the steep gradient region of the ITBs can reach similar values on NSTX as found on devices operating at much higher magnetic fields.

Due to the large momentum input from Neutral Beam Injection (NBI), ion transport on NSTX can be reduced to neoclassical values, consistent with the existing understanding that ion temperature gradient (ITG) microinstability induced transport can be quenched with sufficient $\mathbf{E}\times\mathbf{B}$ flow shear. However, this stabilization does not seem to also effectively suppress transport in the electron channel, resulting in a dominant loss channel through the electrons. In the current work, we explore a new regime of electron confinement where electron temperature profiles are no longer stiff at sufficiently negative magnetic shear. After a general description of the plasmas used in this work, we begin by examining the kinetic profiles of the ITBs followed by a statistical analysis of key profile features. Local electron scale fluctuations inside the ITBs will be examined, and the experimental results will be compared with with gyrokinetic simulations.

Plasma description

Plasmas discussed in this work were all performed at 0.55T, with 1MA of plasma current, using a combination of NBI and High Harmonic Fast Wave (HHFW) radio frequency heating. The L-mode discharges can display a large range of shear reversal, or negative magnetic shear s≡(r/q)dq/dr, during the early portion of the discharge. Figure 1 shows the time evolution of such an ITB discharge, in which an early period of reversed shear, indicated by the elevated $q_0 - q_{min}$, accompanies a rapid rise in the core

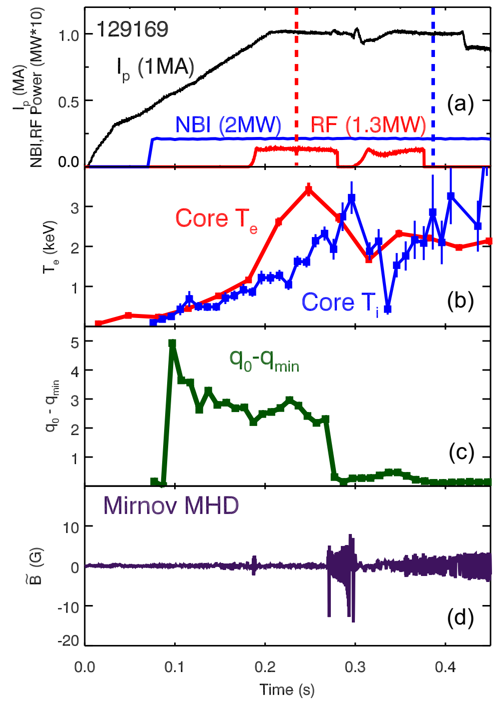

FIG. 1: Time evolution of an initially strongly reversed shear plasma displaying an electron internal transport barrier (e-ITB) until the current redistribution event shown by the MHD trace. (a) plasma current and heating waveforms, (b) core electron and ion temperatures (c) elevated $q_0 - q_{min}$ indicates reversed shear conditions (d) MHD activity. Dashed lines in (a) correspond to times in Figure 2.

electron and ion temperatures, until MHD activity causes the current to redistribute on a timescale much faster than the current relaxation time. The q-profile and toroidal current profile during and after the ITB phase are shown in Figures 2(a) and 2(b). The plasma most often continues with a weakly reversed shear or monotonic q-profile, during which the electon confinement is degraded relative to the shear reversal period, but the ion confinement does not necessarily degrade as significantly.

Profile measurements

A number of diagnostics on NSTX allow for detailed profile measurements, shown in red using the left hand axis in Figure 3 are kinetic profiles from the same plasma as in Figure 1. The electron temperature and density, T_e and n_e, are measured using a 30 channel, 60Hz Thomson scattering system [3]. Ion temperatures, T_i, and toroidal velocity, v_ϕ, are measured using the 51 channel CHarge Exchange Re-

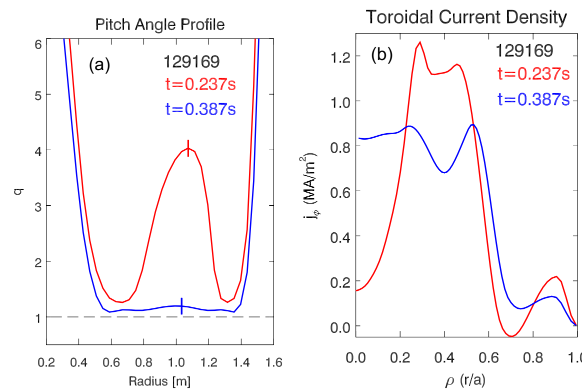

FIG. 2: (a) q and (b) current density profiles during and after the reversed shear period.

combination Spectroscopy (CHERS) [4] with 10ms time resolution. The q-profile is reconstructed using LRDFIT, a free boundary Grad-Shafranov equilibrium reconstruction code that models vacuum vessel eddy currents and makes use of magnetics, electron temperature isothermal flux surfaces, rotation, and E_r corrected pitch angles from a 16 channel Motional Stark Effect (MSE) [5] system with 10ms time resolution.

Normalized gradient scale lengths, $R/L_X \equiv -(R/X)(dX/dr)$, where R is the major radius, are calculated from χ^2 minimized fits to the profile data with spline or tanh functions. Figure 3 shows these normalized gradients in blue using the right hand axis. ITB profiles shows peaked gradients in the core plasma in the electron and ion temperatures, and also in toroidal velocity, while the electron density gradient does not show a dramatic increase with ITB formation. Note that for negative shear q-profiles, s_{min}, the profile magnetic shear minima is a negative quantity, while monotonic q-profiles have $s_{min} = 0$. Figure 3 demonstrates that peak gradients do not necessarily occur at the same radial location.

Comparing the location of profile features requires radial alignment cross-calibration between the profile instruments. In addition to extensive invessel spatial calibrations, CHERS and Thomson scattering radial alignment has been checked using high density H-mode pedestals, where the alignment of the edge pedestal position is observed to agree to within a centimeter [6]. The MSE system in turn shares an optical system with the CHERS diagnostic and therefore no systematic offsets are expected between these diagnostics.

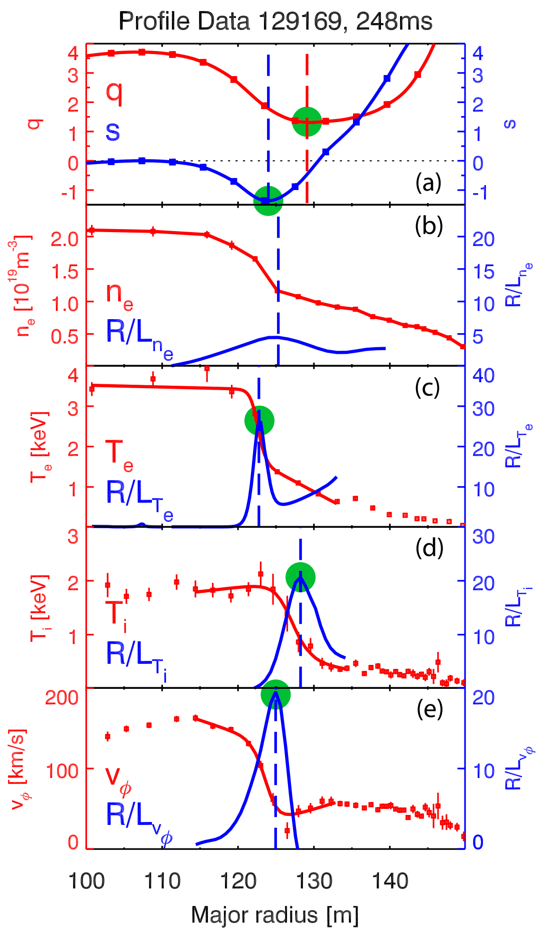

FIG. 3: Kinetic profiles of an ITB. Shown in red using the left hand axes are (a) q, (b) electron density, (c) electron temperature, (d) ion temperature, and (e) toroidal velocity. Shown in blue using the right hand axes are (a) magnetic shear, and (b-e) the normalized gradient scale lengths. Vertical dashed lines and green highlights indicate positions of interest such as q_{min}, s_{min}, peak gradients and their radial locations.

q_{min} and rational q values

Statistical analysis was carried out for a database of over 500 kinetic profiles from over 80 discharges for the value and location of profile features. We begin with a discussion of the relationship between q_{min} and the ITBs.

The location of s_{min} and the ITBs, defined as the radius of peak R/L_{T_e} (e-ITB) and R/L_{T_i} (i-ITB) appears on average 9 cm away from q_{min}, shown as histograms of the occurance fraction within the database in Figure 4. The q values at the ITBs do not favor any particular rational value of q and occurs over a range, as seen in Figure 5. The lack of correlation to rational q values at the transport barriers and the large spatial separation between q_{min} and the ITBs suggests that these are not key factors for NSTX ITBs.

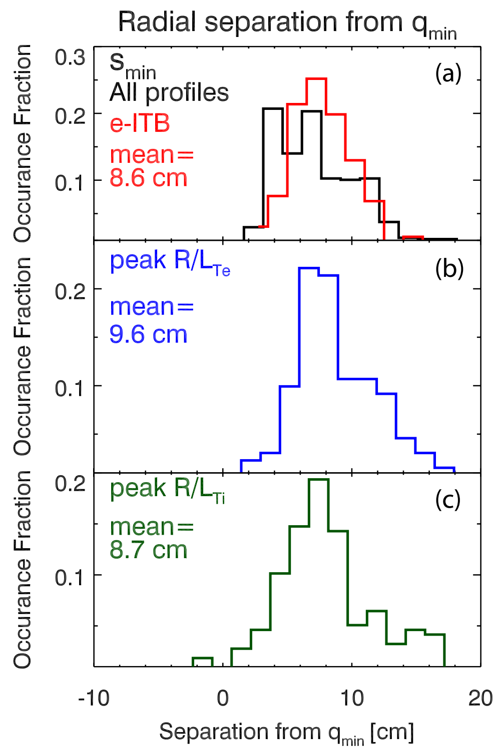

FIG. 4: Distribution of radial separation between q_{min} and (a) s_{min}, for all profiles (black) and e-ITB profiles (red), (b) the e-ITB (c) the i-ITB. Positive spearations indicate that q_{min} occurs radially further outboard.

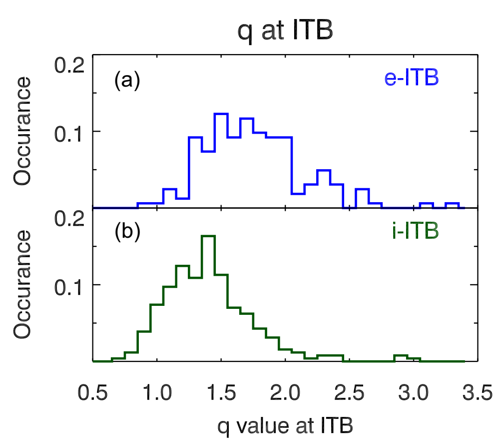

FIG. 5: Distribution of q values at (a) the e-ITBs, (b) the i-ITBs.

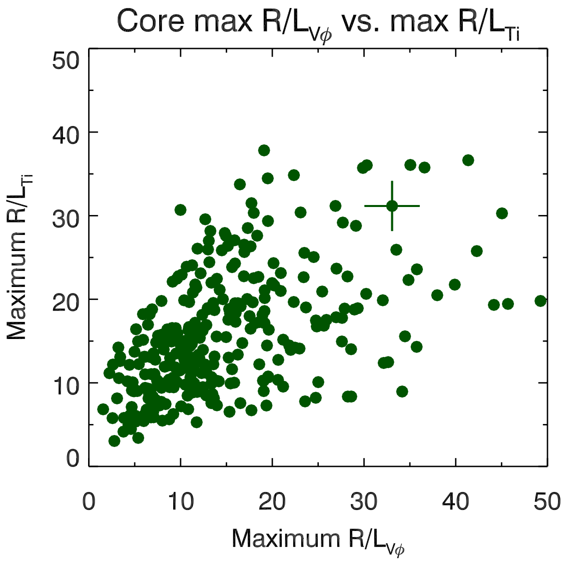

FIG. 6: Peak toroidal velocity gradients, R/L_{v_ϕ} versus peak ion temperature gradients.

Ion Transport Barrier

Ion transport in i-ITBs appears consistent with the general understanding that ITG microturbulence induced transport can be suppressed with sufficient $\mathbf{E} \times \mathbf{B}$ shear. Figure 6 shows a trend of increasing peak R/L_{T_i} with increasing peak R/L_{v_ϕ}, as the toroidal velocity typically provides the largest contribution in the radial force balance equation,

$$E_r = \frac{1}{Z_i e n_i} \nabla P_i - v_{\theta i} B_\phi + v_{\phi i} B_\theta \qquad (1)$$

where $Z_i e$, n_i, P_i are the ion charge, density, and pressure, and v and B are the velocity and magnetic field in the toroidal (ϕ) and poloidal (θ) directions. The large scatter shows that despite stabilization of ion gyroscale modes, the ion temperature gradient is coupled to other factors such as electron transport.

The location of the i-ITB is also well correlated with the location of maximum $\mathbf{E} \times \mathbf{B}$ shear. Figures 7(a) and 7(b) show that the i-ITB statistically occurs most frequently within approximately 3 centimeters of the peak $\mathbf{E} \times \mathbf{B}$ shear position. For the calculation of the $\mathbf{E} \times \mathbf{B}$ shearing rate, the poloidal velocity contribution was neglected due to the lack of calibrated poloidal velocity measurements. This should not effect the results due to the fact that poloidal flows and their gradients are expected to be small in the core, based on neoclassical calculations from NCLASS [7]. Linear gyrokinetic simulations [8] show ion gyroscale modes to be stable in ITB profiles.

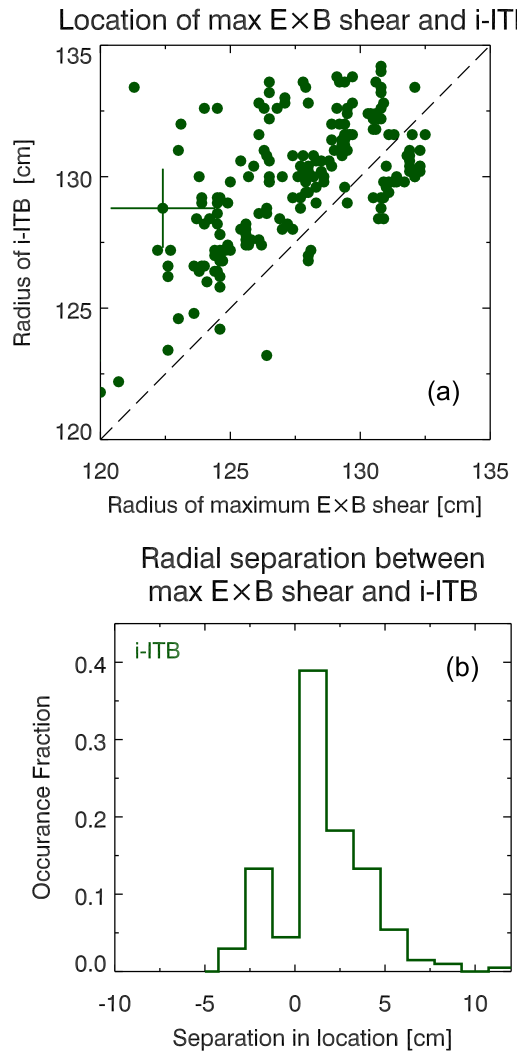

FIG. 7: (a) Radius of the i-ITB compared to the location of maxium $\mathbf{E} \times \mathbf{B}$ shear, shown with equality line. (b) Histogram of radial separation between i-ITB and location of maxium $\mathbf{E} \times \mathbf{B}$ positive values indicate i-ITB is radially outwards.

Electron Transport Barrier

From the profiles shown in Figure 3, one can see that the e-ITB does not necessarily occur at the i-ITB location. The location of the e-ITB best correlates with the location of minimum magnetic shear. Figure 8(a) shows the radius of the e-ITBs versus the radius of s_{min} and a histogram of their separation distance is shown in Figure 8(b). The e-ITB occurs almost exclusively at s_{min} or a few centimeters inboard. Overlaid in the same figure, one can see the separation between the i-ITB and s_{min} is in the oppposite direction, with the i-ITB occuring mostly outboard of the s_{min} location, and better correlated with the location of the peak of the $\mathbf{E} \times \mathbf{B}$ shearing rate. These results are consistent with the general understanding that $\mathbf{E} \times \mathbf{B}$ shear can effectively suppress ITG induced ion turbulence, but that magnetic shear plays a more important role in electron transport suppression.

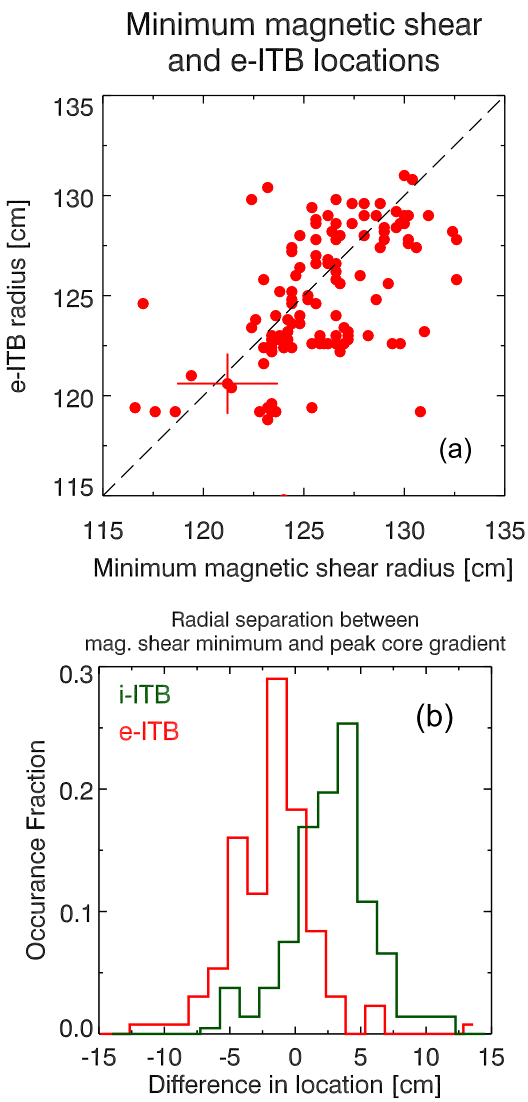

FIG. 8: (a) Radius of the e-ITB vs. radius of s_{min}.. (b) Histogram of radial separation between s_{min} and the e-ITB (red) and i-ITBs (green). Positive values indicate ITB is radially outwards from s_{min}.

The transition out of the stiff T_e profile regime due to sufficiently negative magnetic shear is shown

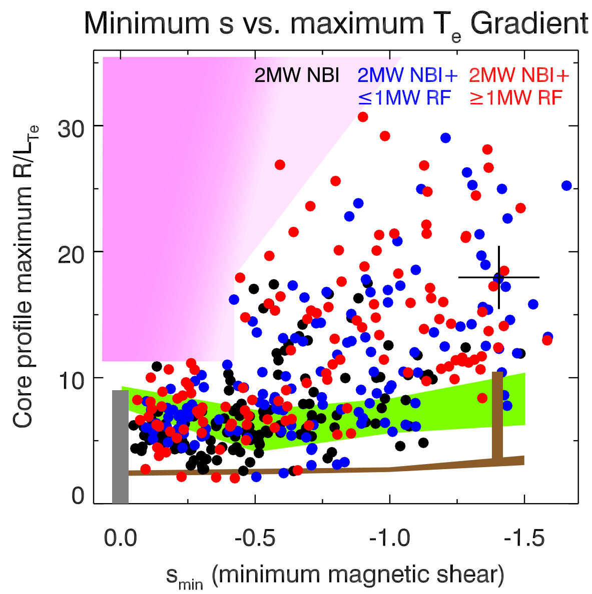

FIG. 9: Value of minimum magnetic shear vs. peak electron temperature gradient. Shaded region in the upper left shows an inaccessible region due to stiff profiles. Horizontal bands in green and brown show critical ETG gradients. Grey vertical band at $s_{min} = 0$ serve as a reference from high β H-mode discharges.

in Figure 9, in which the peak core R/L_{T_e} is plotted against s_{min} for increasing auxilliary heating power, from 2 MW NBI (black), to 2 MW NBI with up to 1 MW of HHFW (blue), and 2 MW NBI with greater than 1 MW of HHFW (red). A reference range for typically observed core gradients in NSTX is shown by the vertical grey region at $s_{min} = 0$, using high input power (6MW NBI), high-β H-modes with monotonic q-profiles. Data in Figure 9 were not specifically filtered for peak gradient times, and shows a large range of values at each value of magnetic shear. While many points may reflect still developing e-ITBs and others do not reach high R/L_{T_e} due to insufficient heating power or ion thermal transport, there are a few discharges that do not develop steep electron temperature gradients despite having sufficient negative shear and input power.

The data shown in Figure 9 spans a range of plasma parameters. Plasma density variation at the e-ITB range from 1 to $4\times10^{19}\mathrm{m}^{-3}$, with Z_{eff} ranging from 1.1 to 4 due to the use of both deuterium and helium as the bulk plasma species and varying wall conditions. Various levels of lithium evaporation wall conditioning [9] were also employed during the experiment, primarily to control densities near the RF antennas to optimize coupling. Additionally, the ratio of T_e/T_i ranges from 0.4 to 2.5 at the e-ITB location. These parameter ranges, which exist at both high and low magnetic shears, were examined but did not correlate well to electron temperature gradients.

The inability to access high R/L_{T_e} at zero or weakly reversed magnetic shear with additional heating power, shown as the shaded upper left region in Figure 9, reveals that for $s_{min} \geq -0.4$, the T_e profile is stiff and limited to $R/L_{T_e} < 11$. However, profiles with $s_{min} < -0.4$ appear to be in a different regime, where electron temperature gradients can be increased to large values using the same level of input power. The data suggests that in the intermediate shear region, $-0.4 \geq s_{min} \geq -1.0$, the maximum sustainable gradient may be a function of s_{min}, but more datapoints at even higher input power would be needed to confirm this. Horizontal regions in green and brown in Figure 9 showing critical gradients for electron modes will be discussed when these measurements are compared to simulations.

The combined effect of simultaneous electron and ion ITBs is shown in Figure 10, showing ion thermal diffusivities near the neoclassical value at the i-ITB. Electron thermal diffusivities below that of the ions is typically not observed without a strong e-ITB, with typical χ_e values observed in weakly reversed shear discharges ranging between 10-20 m^2/s [5].

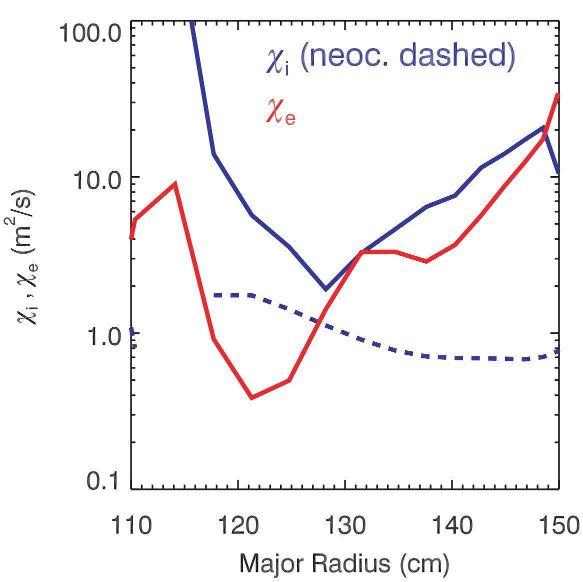

FIG. 10: TRANSP calculations of the electron and ion thermal diffisivities with an ITB. Magnetic axis (not shown) is at 102 cm, and the plasma edge is at 154 cm.

Electron fluctuation measurements

Having established a connection between negative magnetic shear and the ability to sustain higher electron temperature gradients, a microwave scattering diagnostic was used to measure local electron density fluctuations at the e-ITB at electron scale wavenumbers ($k_\perp \rho_e \leq 0.6$) [10, 11, 12].

Figure 11(a) compares fluctuation power spectra between two discharges, one that is weakly reversed shear q-profile without an e-ITB (red) and a strongly reversed shear with an e-ITB (blue). The T_e profiles and q-profiles are shown in corresponding colors in Figures 11(b) and (c). The high-k fluctuations for the negative magnetic shear case are lower in amplitude over a wide frequency range despite elevated electron temperature gradients ($R/L_{T_e} \geq 20$).

Fluctuation measurements were also taken outside the region of negative magnetic shear, near the location of q_{min}, where the magnetic shear is zero. Measurements at this location did not display the same suppression of fluctuation regardless of the value of magnetic shear further inside the plasma, illustrating that turbulence suppression is a local phenomenon tied to the local magnetic shear value.

Examples of e-ITBs up until this point have used NBI for both heating and diagnostic purposes. Despite evidence showing that magnetic shear is the more important factor for electron transport, $\mathbf{E} \times \mathbf{B}$ shear has nonetheless been present. Figure 12(a) shows a comparison of high-k fluctuation spectra between two discharges heated only with HHFW, using 50ms NBI blips for diagnosis. The electron temperature profiles and q-profiles are shown in Figure 12(b) and (c), with similar results as beam heated e-ITBs, where the strongly reversed shear discharge with steep T_e gradients shows reduced fluctuations. E_r and the $\mathbf{E} \times \mathbf{B}$ shearing rate for the e-ITB case are shown in Figure 12(a) and 12(b). The lack of $\mathbf{E} \times \mathbf{B}$ shear around the fluctuation measurement region shows that magnetic shear alone is capable of suppressing electron scale fluctuations. This calculation also excludes the poloidal velocity, which is expected to contribute minimally to the $\mathbf{E} \times \mathbf{B}$ shear in the plasma core.

Fluctuation power was statistically analyzed and shown in Figures 14 where the fluctuation power was integrated over frequency for 5 ms periods immediately preceeding each kinetic profile for two high-k channels. Due to local T_e variation at the measurement location, not every measurement point is identical in $k_\perp \rho_e$. However, the fact that both high-k channels at different wavenumbers show sim-

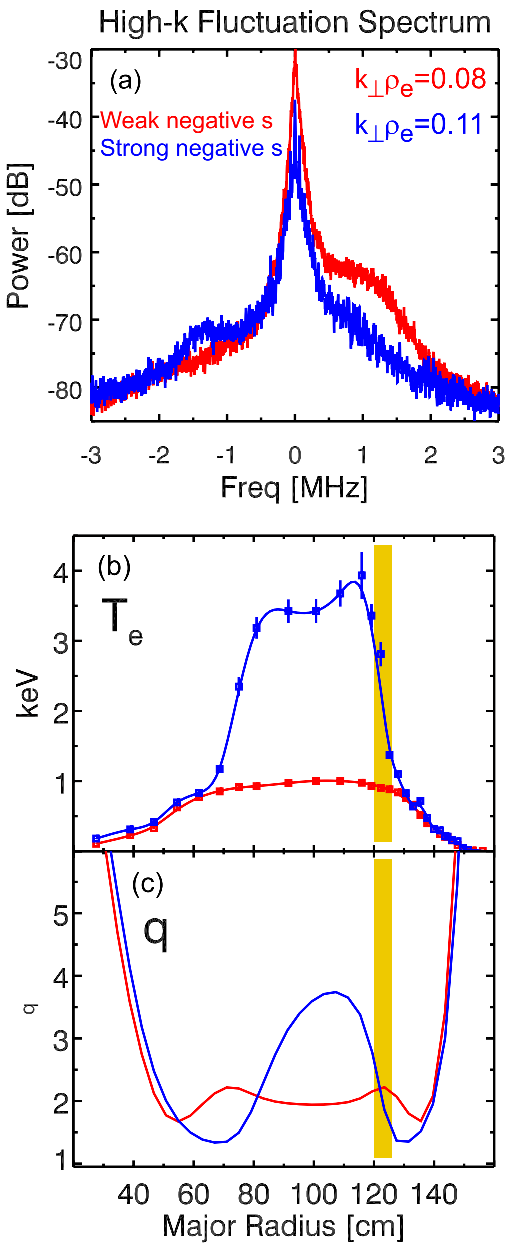

FIG. 11: (a) High-k microwave scattering fluctation power spectra comparison between a case with an e-ITB and strongly negative magnetic shear (red) vs. a weakly reversed shear case with lower electron temperature gradients (blue). (b) Electron temperatures and (c) q-profiles for cases shown in (a), shaded region indicates the high-k measurement region.

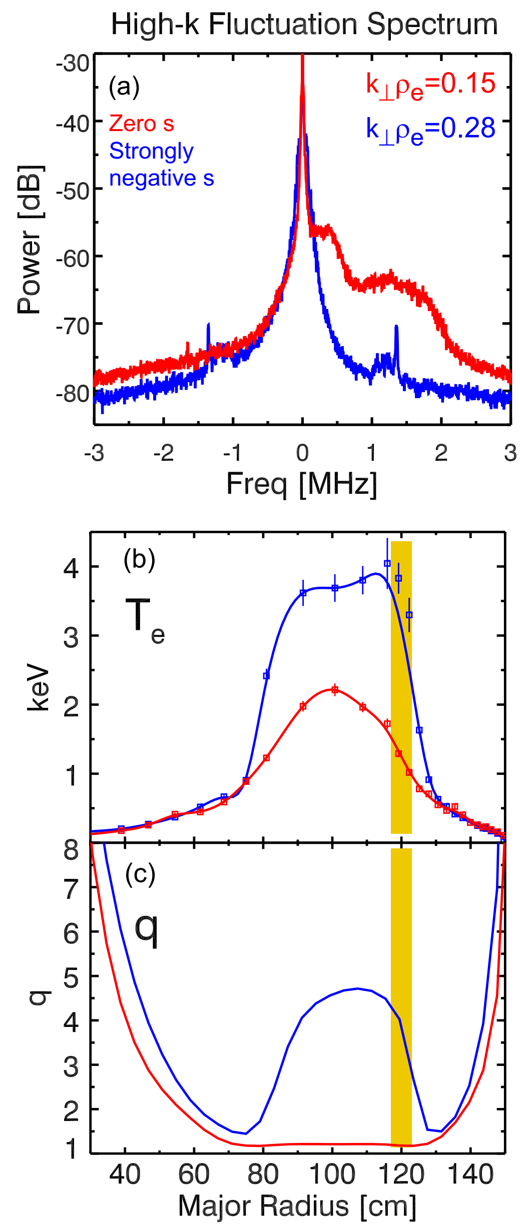

FIG. 12: (a) High-k fluctation power spectra comparing two RF heated cases, (red) shows a reversed shear e-ITB case, while (blue) shows a zero shear case. (b) Electron temperatures and (c) q-profiles for cases shown in (a), shaded region indicates the high-k measurement region.

ilar results suggests that fluctuations are suppressed over a range of wavenumbers. While a large range of fluctuation power exist for the zero or weakly reversed sheared plasmas, this could be explained by variations in critical gradients for electron gyroscale modes due to varying plasma parameters. A trend can be seen towards increasing fluctuation power with increasing electon temperature gradi-

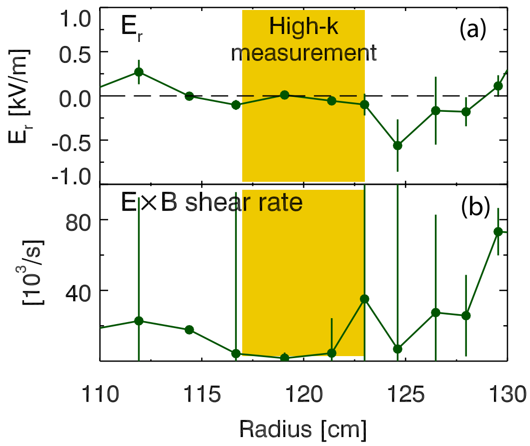

FIG. 13: (a) E_r at the high-k measurement region (b)$\mathbf{E}\times\mathbf{B}$ shearing rate at the high-k measurement region.

ents, though with significant scatter. What is clear, however, is that strongly reversed sheared e-ITBs display lower levels of integrated fluctuation power, by about an order of magnitude, across a range of $k_\perp\rho_e$ despite having significantly higher electon temperature gradients.

Comparison to gyrokinetic simulations

Linear gyrokinetic simulations were used to calculated critical temperature gradients, $(R/L_{T_e})_{crit}$, for the onset of electron thermal gradient (ETG) modes over the range of measured magnetic shears and electron temperature gradients. For GS2 simulations [13], critical gradients were calculated for sample experimental profiles with and without ITBs. The calculated range is shown by the shaded green band in Figure 9. The brown bands in the same figure show results from linear GYRO simulations [8, 14], where a single ITB profile was used but the parameters $\tau = Z_{eff}T_e/T_i$ and the magnetic shear were varied in the simulations to account for the variations observed in the experiments. Because the ETG $(R/L_{T_e})_{crit}$ does not change significantly with increasingly negative magnetic shear, these results show that the measured electron temperature gradient can greatly exceed critical ETG gradients, but only for strongly negative magnetic shear.

The connection between high-k fluctuations on NSTX and ETG microinstabilities has been previously established in [15], and the currently observed reduction in fluctuation levels are consistent with previous works from [16], where nonlinear gyrokinetic simulation results showed that electron thermal transport due to ETG modes would be significantly reduced at strongly negative magnetic shears.

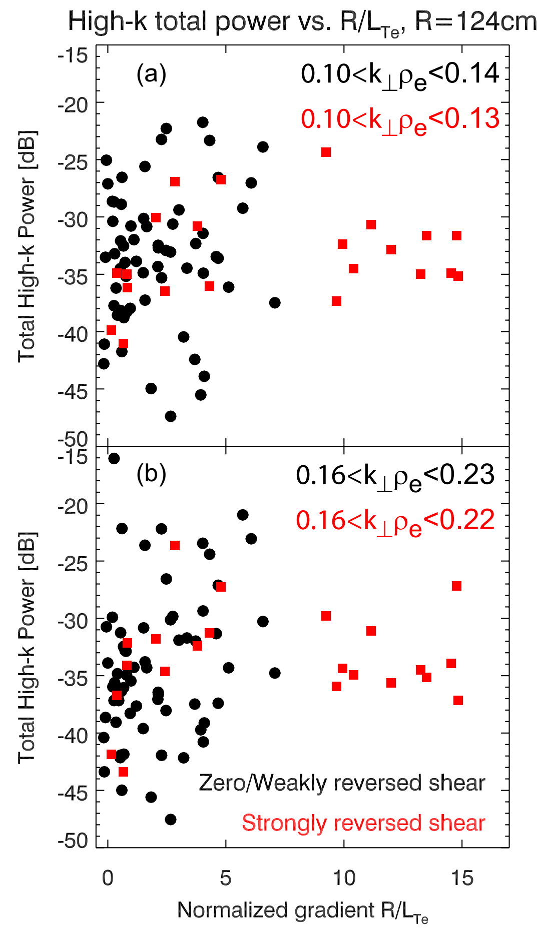

FIG. 14: Integrated high-k power statistics at two ranges of $k_\perp\rho_e$ vs. the local R/L_{T_e} at the flucutation measurement location. $k_\perp\rho_e$ variation is due to changes in T_e at the measurement location.

Conclusion

In conclusion, we have observed internal transport barriers in NSTX for reversed shear discharges in the electron thermal, ion thermal, and toroidal velocity channels. Statistical analysis of a kinetic profile database shows that the i-ITB is best correlated with the location of maximum $\mathbf{E}\times\mathbf{B}$ shear and the related to the value of the toroidal velocity shear. The e-ITB, on the other hand, is best correlated with s_{min} and can show a transition out of a stiff profile regime when the magnetic shear reaches a sufficiently negative value. Density fluctuation measurements at the electron gyroscale in the steep gradient region of the e-ITB show reduced fluctuation levels despite greatly exceeding the ETG $(R/L_{T_e})_{crit}$ relative to zero and weakly sheared profiles. The combination of e-ITB and i-ITBs results in significantly reduced thermal diffusivities.

We are grateful for the support and hard work from the NSTX team and PPPL. This research is supported by U.S. DOE Grant No. DE-FG02-99ER54520 and U.S. DOE Contract No. DE-AC02-76CH03073.

* hyuh@pppl.gov

[1] J. Connor, T. Fukuda, X. Garbet, C. Gormezano, V. Mukhovatov, M. Wakatani, the ITB Database Group, the ITPA Topical Group on Transport, and I. B. Physics, Nuclear Fusion **44**, R1 (2004).

[2] H. Meyer, A. R. Field, R. J. Akers, C. Brickley, N. J. Conway, A. Patel, P. G. Carolan, C. Challis, G. F. Counsell, G. Cunningham, et al., Plasma Physics and Controlled Fusion **46**, A291 (2004).

[3] B. P. LeBlanc, R. E. Bell, D. W. Johnson, D. E. Hoffman, D. C. Long, and R. W. Palladino, Papers from the 14th Topical Conference on High Temperature Plasma Diagnostics **74**, 1659 (2003).

[4] R. Bell, D. Johnson, R. Feder, and T. Biewer, Bulletin of the 47th annual meeting of the division of plasma physics of the American Physical Society **50**, RP1.005 (2005).

[5] F. M. Levinton, H. Yuh, M. G. Bell, R. E. Bell, L. Delgado-Aparicio, M. Finkenthal, E. D. Fredrickson, D. A. Gates, S. M. Kaye, B. P. LeBlanc, et al., Physics of Plasmas **14**, 056119 (pages 9) (2007).

[6] B. LeBlanc and R. Bell, private communication (2008).

[7] W. A. Houlberg, K. C. Shaing, S. P. Hirshman, and M. C. Zarnstorff, Physics of Plasmas **4**, 3230 (1997).

[8] J. Peterson, G. Hammett, D. Mikkelsen, S. Kaye, J. Candy, and R. E. Waltz, Bulletin of the 50th annual meeting of the division of plasma physics of the American Physical Society **50**, NP6.096 (2008).

[9] H. Kugel, M. Bell, R. Bell, C. Bush, D. Gates, T. Gray, R. Kaita, B. Leblanc, R. Maingi, R. Majeski, et al., Journal of Nuclear Materials **363-365**, 791 (2007), plasma-Surface Interactions-17.

[10] E. Mazzucato, Physics of Plasmas **10**, 753 (2003).

[11] D. R. Smith, E. Mazzucato, T. Munsat, H. Park, D. Johnson, L. Lin, C. W. Domier, M. Johnson, and J. N. C. Luhmann, Review of Scientific Instruments **75**, 3840 (2004).

[12] D. R. Smith, E. Mazzucato, W. Lee, H. K. Park, C. W. Domier, and J. N. C. Luhmann, Review of Scientific Instruments **79**, 123501 (2008).

[13] M. Kotschenreuther, G. Rewoldt, and W. M. Tang, Computer Physics Communications **88**, 128 (1995).

[14] J. Candy and R. E. Waltz, Journal of Computational Physics **186**, 545 (2003).

[15] E. Mazzucato, D. R. Smith, R. E. Bell, S. M. Kaye, J. C. Hosea, B. P. LeBlanc, J. R. Wilson, P. M. Ryan, C. W. Domier, J. N. C. Luhmann, et al., Physical Review Letters **101**, 075001 (pages 4) (2008).

[16] F. Jenko and W. Dorland, Phys. Rev. Lett. **89**, 225001 (2002).